

Optimal Time-Domain Pulse Width Modulation for Three-Phase Inverters

Siddharth Tyagi and Isaak Mayergoyz

*Electrical and Computer Engineering,
University of Maryland, College Park, MD, 20740, USA*

Abstract

A novel optimal time-domain technique for pulse-width modulation (PWM) in three-phase inverters is presented. This technique is based on the time-domain per phase analysis of three-phase inverters. The role of symmetries on the structure of three-phase PWM inverter voltages and their harmonic contents are discussed. Numerical results highlighting improvements in the harmonic performance of three-phase inverters are presented.

I. INTRODUCTION

Inverters are power electronics circuits which convert DC input voltages into sinusoidal AC output voltages and currents of desired and controllable frequencies. They are widely used in many applications, such as speed control of AC motors in variable-frequency drives (VFDs) [1–3], uninterruptible power supplies (UPS) [5, 6] and for the integration of renewable energy sources with the grid [7–9]. Pulse width modulation (PWM) is mainly used to generate output AC voltages in inverters [1–3, 10]. The principle of PWM is to generate inverter voltages which are trains of rectangular pulses. The widths of these pulses are properly modulated to suppress lower-order voltage

harmonics at the expense of higher order harmonics. Then, the higher order harmonics are suppressed in output currents and voltages by inductors in the inverter circuit.

Usually, the H-bridge topology shown in Fig. 1 is used in the design of three-phase inverters. There are a number of ways to generate pulse width modulated voltages and currents for the three-phase circuit inverter shown in Fig. 1. Space Vector PWM (SVPWM) is the most commonly used method to generate PWM pulses for such inverters [1, 13]. Over the years, extensive research has been performed on optimal PWM in the frequency domain, that improves upon the SVPWM technique [14]- [21]. In parallel, PWM has been used to selectively eliminate lower-order harmonics. This technique is usually termed as Selective Harmonic Elimination (SHE) and has been extensively studied in the literature [22–25, 27–30]. Other optimal PWM methods based in different ideas have been explored as well [31–33].

The above referenced publications on PWM are concerned with the frequency harmonic content of line-voltages in three phase inverters. In contrast, the emphasis in this paper is on the harmonic contents of phase currents or voltages across the resistors shown in Fig. 1. This is achieved by using the time-domain per-phase analysis to find analytical expressions for phase currents, which are then used for minimization of their harmonic-contents. Furthermore, in the framework of the developed technique, specific lower-order harmonics can be completely eliminated by imposing certain constraints on the minimization problem. In this way, SHE is achieved simultaneously with minimization of Total Harmonic Distortion (THD).

This manuscript is organized as follows. In Section II, we present a time-domain analysis of PWM for three-phase inverters. The PWM voltages are fully characterized by switching time-instants. The exact analytical solutions for currents and voltages in the circuit shown in Fig. 1 can be obtained in terms of these time-instants. By using these analytical solutions, the problem of optimal PWM design can be framed as a minimization problem.

Symmetries play an important role in the formation of PWM line-voltages in three-phase inverters. In Section III, we discuss the mathematical and physical aspects of

symmetries involved in the performance of PWM inverters. It turns out that these symmetries considerations impose specific constraints on the switching time-instants that describe PWM three-phase line-voltages. In Sections IV, some mathematical details of the optimization technique are discussed, and numerical results are presented.

II. TIME-DOMAIN ANALYSIS

A. Per-Phase Analysis of Three-Phase Inverter

A three-phase H-bridge inverter is shown in Fig. 1. Here, V_0 is the DC input voltage. The 3-phase Y-type load connected to the inverter is modeled by using inductors (L) and resistors (R). It is assumed that the load is balanced.

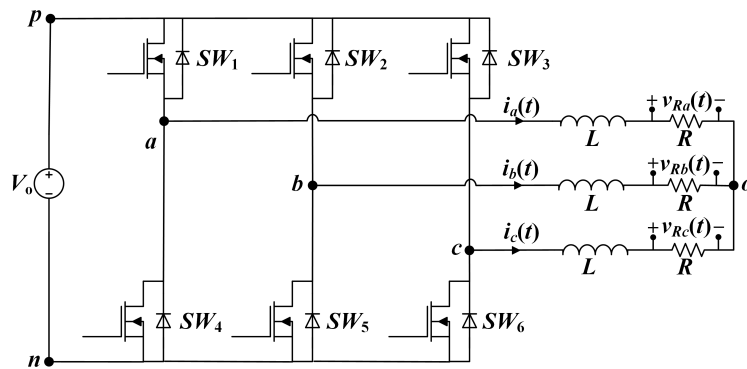


Figure 1: 3-phase H-Bridge Inverter

We now proceed to derive per-phase equations for the inverter. Using KVL, we find from Fig. 1 that the phase-currents $i_a(t)$, $i_b(t)$ and $i_c(t)$ satisfy the following equations:

$$L \frac{di_a}{dt}(t) + Ri_a(t) = v_a(t) - v_o(t), \quad (1)$$

$$L \frac{di_b}{dt}(t) + Ri_b(t) = v_b(t) - v_o(t), \quad (2)$$

$$L \frac{di_c}{dt}(t) + Ri_c(t) = v_c(t) - v_o(t), \quad (3)$$

where $v_a(t)$, $v_b(t)$, $v_c(t)$ and $v_o(t)$ are potentials of nodes a , b , c and o , respectively, measured with respect to some reference node, for instance, node n . Similarly, using KCL,

we find

$$i_a(t) + i_b(t) + i_c(t) = 0. \quad (4)$$

Adding equations (1), (2) and (3) and using (4), we get the following expression for $v_o(t)$:

$$v_o(t) = \frac{v_a(t) + v_b(t) + v_c(t)}{3}. \quad (5)$$

By substituting the last equation into equation (1), we find:

$$\begin{aligned} L \frac{di_a}{dt}(t) + Ri_a(t) &= v_a(t) - \frac{v_a(t) + v_b(t) + v_c(t)}{3} \\ &= \frac{2}{3}v_a(t) - \frac{1}{3}[v_b(t) + v_c(t)] \\ &= \frac{1}{3}[v_a(t) - v_b(t) + v_a(t) - v_c(t)]. \end{aligned} \quad (6)$$

Thus,

$$L \frac{di_a}{dt}(t) + Ri_a(t) = \frac{1}{3}[v_{ab}(t) + v_{ac}(t)]. \quad (7)$$

Similarly, we can derive:

$$L \frac{di_b}{dt}(t) + Ri_b(t) = \frac{1}{3}[v_{bc}(t) + v_{ba}(t)], \quad (8)$$

$$L \frac{di_c}{dt}(t) + Ri_c(t) = \frac{1}{3}[v_{ca}(t) + v_{cb}(t)]. \quad (9)$$

We note here that the right-hand sides of equations (7), (8) and (9) depend on the PWM line-voltages which are generated by the inverter, while the left-hand sides of the above equations contain the phase-currents. Thus, (7), (8) and (9) can be interpreted as the per-phase model of the inverter. These equations shall be used to derive the analytical solution of the phase-currents, and optimize the harmonic-performance of the inverter. It is instructive to highlight the following similarity of the above time-domain per-phase model of the inverter to the frequency domain per-phase analysis of 3-phase AC circuits under balanced operation. Indeed, once we obtain the analytical solution for the phase current $i_a(t)$ from equation (7) [as discussed in the next section], the analytical expressions for $i_b(t)$ and $i_c(t)$ are easily obtained as versions of $i_a(t)$ time-shifted by $\frac{T}{3}$ and $\frac{2T}{3}$, respectively. This is the essence of per-phase analysis, where

solution for currents and voltages in one phase yields the complete information about currents and voltages in other phases by appropriate time-shifts.

It is interesting to point out that the right-hand sides of per-phase equations (7)-(9) are two-level voltages produced by single-level pulse width modulated line-voltages $v_{ab}(t)$, $v_{bc}(t)$ and $v_{ca}(t)$. This is in clear contrast with single-phase PWM inverters, where the currents are driven by single level line-voltages.

B. Analytical Expression for Phase Currents

For three-phase inverters, the line-voltages are periodic trains of rectangular pulses, as shown in Fig. 2. Let T be the time-period of these voltages, and the associated frequency be $\omega = \frac{2\pi}{T}$. If the number of pulses in the interval $(0, \frac{T}{2})$ is N , then these rectangular pulses can be described by a sequence of strictly monotonically increasing switching time-instants t_1, t_2, \dots, t_{2N} .

We shall now proceed to derive the expressions for the phase currents $i_a(t)$, $i_b(t)$ and $i_c(t)$ as functions of these switching time-instants. Let $i_{ab}(t)$ and $i_{ac}(t)$ be solutions to the following equations:

$$L \frac{di_{ab}}{dt}(t) + Ri_{ab}(t) = v_{ab}(t), \quad (10)$$

$$L \frac{di_{ac}}{dt}(t) + Ri_{ac}(t) = v_{ac}(t). \quad (11)$$

Then, according to the superposition principle for linear differential equations, the solution $i_a(t)$ to equation (7) can be written as:

$$i_a(t) = \frac{1}{3} [i_{ab}(t) + i_{ac}(t)]. \quad (12)$$

Similar expressions can be written for the other phase currents.

We begin by solving equation (10) for $i_{ab}(t)$ in terms of the switching time-instants that describe the line-voltage $v_{ab}(t)$. Let $v_{ab}(t)$ be a train of rectangular pulses as shown in Fig. 2, and hence it can be described by the time-instants t_1, t_2, \dots, t_{2N} . The voltage

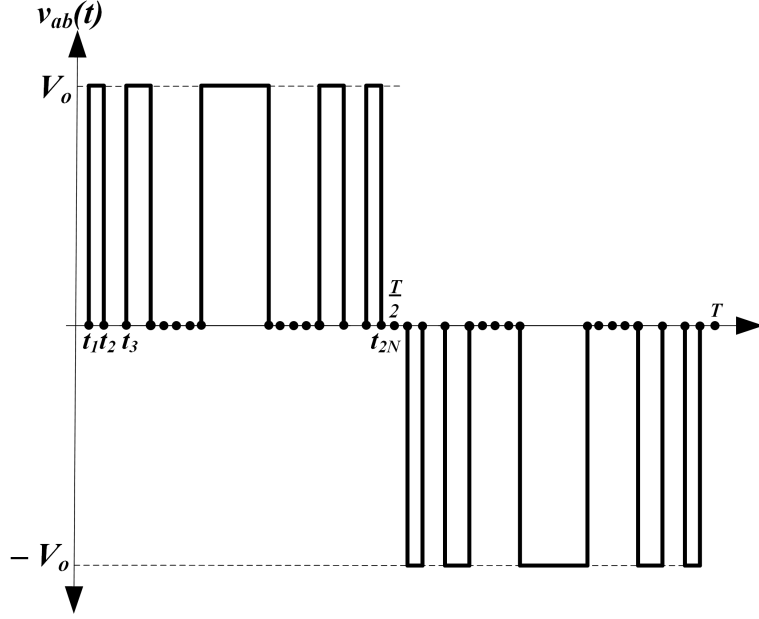


Figure 2: Structure of Output Line-Voltage

$v_{ab}(t)$ must have half-wave symmetry to eliminate even harmonics. This means that:

$$v_{ab}\left(t + \frac{T}{2}\right) = -v_{ab}(t). \quad (13)$$

Thus, $v_{ab}(t)$ can be completely characterized by its values in the interval $0 \leq t \leq \frac{T}{2}$.

It is clear that the following formula is valid for $v_{ab}(t)$:

$$v_{ab}(t) = \begin{cases} 0, & \text{if } t_{2j} < t < t_{2j+1}, \\ V_0, & \text{if } t_{2j+1} < t < t_{2j+2}, \end{cases} \quad (14)$$

where $j = 0, 1, 2, \dots, N$, and

$$t_0 = 0, \quad t_{2N+1} = \frac{T}{2}. \quad (15)$$

From equations (10) and (14), we find that:

$$i_{ab}(t) = \begin{cases} A_{2j+1}e^{-\frac{R}{L}t}, & \text{if } t_{2j} < t < t_{2j+1}, \\ A_{2j+2}e^{-\frac{R}{L}t} + \frac{V_0}{R}, & \text{if } t_{2j+1} < t < t_{2j+2}, \end{cases} \quad (16)$$

where the constants A_{2j+1} and A_{2j+2} must be determined by using the continuity of electric current $i_{ab}(t)$ at times t_{2j} and t_{2j+1} as well as the half-wave symmetry boundary

condition:

$$i_{ab}\left(\frac{T}{2}\right) = -i_{ab}(0), \quad (17)$$

imposed by the half-wave symmetry [see equation (13)] of $v_{ab}(t)$.

From formula (16), using the continuity of $i_{ab}(t)$ at the time-instants t_1, t_2, \dots, t_{2N} , as well as the boundary condition (17), we arrive at the following simultaneous equations:

$$A_2 - A_1 = -\frac{V_0}{R} e^{\frac{Rt_1}{L}}, \quad (18)$$

$$A_3 - A_2 = \frac{V_0}{R} e^{\frac{Rt_2}{L}}, \quad (19)$$

⋮

$$A_{2j} - A_{2j-1} = -\frac{V_0}{R} e^{\frac{Rt_{2j-1}}{L}}, \quad (20)$$

$$A_{2j+1} - A_{2j} = \frac{V_0}{R} e^{\frac{Rt_{2j}}{L}}, \quad (21)$$

⋮

$$A_{2N+1} - A_{2N} = \frac{V_0}{R} e^{\frac{Rt_{2N}}{L}}, \quad (22)$$

and

$$A_1 + A_{2N+1} e^{-\frac{RT}{2L}} = 0. \quad (23)$$

These are linear simultaneous equations with a sparse two-diagonal matrix. These equations can be analytically solved as follows. Adding all the equations from (18) to (22), we find

$$A_{2N+1} - A_1 = \frac{V_0}{R} \sum_{j=1}^{2N} (-1)^j e^{\frac{Rt_j}{L}}. \quad (24)$$

Solving equations (23) and (24), we derive:

$$A_{2N+1} = \frac{V_0 \sum_{j=1}^{2N} (-1)^j e^{\frac{Rt_j}{L}}}{R (1 + e^{-\frac{RT}{2L}})}, \quad (25)$$

$$A_1 = -\frac{V_0 \sum_{j=1}^{2N} (-1)^j e^{\frac{Rt_j}{L}}}{R (1 + e^{-\frac{RT}{2L}})} e^{-\frac{RT}{2L}}. \quad (26)$$

Having found A_1 all other A -coefficients can be computed using the following formula:

$$A_j = A_1 + \frac{V_0}{R} \sum_{n=1}^{j-1} (-1)^n e^{\frac{R}{L} t_n} \quad \text{for } j = 2, 3, \dots, 2N. \quad (27)$$

The above formula is obtained by adding the first $j - 1$ equations (18)-(22).

By using the above formulas for the A -coefficients in equation (16), we find the general analytical solution for the current $i_{ab}(t, t_1, t_2, \dots, t_{2N})$ in terms of the switching time-instants that describe the voltage $v_{ab}(t)$.

Next, we find the analytical expression for $i_{ac}(t)$. We observe that, in order to eliminate all harmonics of orders divisible by three in the line-voltages, the following translational-symmetry condition must be satisfied:

$$v_{ab}(t) = v_{bc}\left(t + \frac{T}{3}\right) = v_{ca}\left(t - \frac{T}{3}\right). \quad (28)$$

Furthermore,

$$\begin{aligned} v_{ba}(t) &= -v_{ab}(t), \\ v_{cb}(t) &= -v_{bc}(t), \\ v_{ac}(t) &= -v_{ca}(t). \end{aligned}$$

The above two equations imply that $i_{ac}(t)$ is a time-shifted version of $i_{ab}(t)$. Namely, $i_{ac}(t)$ can be expressed as a function of the switching time-instants t_1, t_2, \dots, t_{2N} as follows:

$$i_{ac}(t, t_1, \dots, t_{2N}) = -i_{ab}\left(t + \frac{T}{3}, t_1, \dots, t_{2N}\right). \quad (29)$$

Substituting the analytical expression for $i_{ab}(t)$ given by equations (16) and (25)-(27) as well as equation (29) in equation (12), we arrive at the following expression for $i_a(t)$:

$$\begin{aligned} i_a(t) &= \frac{1}{3} \left[i_{ab}(t, t_1, t_2, \dots, t_{2N}) \right. \\ &\quad \left. - i_{ab}\left(t + \frac{T}{3}, t_1, t_2, \dots, t_{2N}\right) \right]. \end{aligned}$$

The latter implies that:

$$i_a(t) = i_a(t, t_1, t_2, \dots, t_{2N}), \quad (30)$$

which means that the analytical expression for the phase-current $i_a(t)$ in terms of the switching time-instants t_1, t_2, \dots, t_{2N} that describe three-phase line-voltages can be obtained.

Before proceeding with the further discussion, we make the following important observation. Equations (28) and (29) imply that all three-phase line-voltages can be described by a *single* sequence of strictly monotonically increasing switching time-instants t_1, t_2, \dots, t_{2N} . However, it turns out that not any given sequence of strictly monotonically increasing time-instants t_1, t_2, \dots, t_{2N} may, in general, represent three-phase PWM line-voltages. The reason is that time-symmetries of line voltages, as well as the KVL requirement that the voltages $v_{ab}(t)$, $v_{bc}(t)$ and $v_{ca}(t)$ must add up to zero, impose specific constraints on the switching time-instants that describe 3-phase PWM line-voltages. Furthermore, there are also constraints imposed by the fact that only two switches in the same leg of the three-phase inverter in Fig. 1 are usually operated simultaneously. The detailed discussion of these constraints is presented in section III.

C. Time-Domain Optimization

Now, we shall describe the central idea of the optimal time-domain pulse width modulation technique.

We begin with deriving the expression for the fundamental harmonic component of $i_a(t)$. The fundamental harmonic components of the line-voltages $v_{ab}(t)$, $v_{bc}(t)$ and $v_{ca}(t)$ can be written as follows:

$$v_{ab,1}(t) = V_m \sin(\omega t), \quad (31)$$

$$v_{bc,1}(t) = V_m \sin\left(\omega t - \frac{2\pi}{3}\right), \quad (32)$$

$$v_{ca,1}(t) = V_m \sin\left(\omega t + \frac{2\pi}{3}\right). \quad (33)$$

Using equations (10) and (11), along with (29), (31) and (33), the corresponding funda-

mental harmonic components of currents $i_{ab}(t)$ and $i_{ac}(t)$ can be expressed as follows:

$$i_{ab,1}(t) = \frac{V_m}{\sqrt{R^2 + (\omega L)^2}} \sin(\omega t - \phi), \quad (34)$$

$$i_{ac,1}(t) = -\frac{V_m}{\sqrt{R^2 + (\omega L)^2}} \sin\left(\omega t + \frac{2\pi}{3} - \phi\right), \quad (35)$$

where

$$\tan \phi = \frac{\omega L}{R}. \quad (36)$$

By using equations (34) and (35) as well as formula (12), the fundamental harmonic component of $i_a(t)$ can be obtained. Namely,

$$i_{a,1}(t) = \frac{V_m}{\sqrt{3}\sqrt{R^2 + (\omega L)^2}} \sin\left(\omega t - \phi - \frac{\pi}{6}\right), \quad (37)$$

which can also be written as:

$$i_{a,1}(t) = I_m \sin\left(\omega t - \phi - \frac{\pi}{6}\right), \quad (38)$$

where

$$V_m = \sqrt{3}I_m\sqrt{R^2 + (\omega L)^2}. \quad (39)$$

Next, we want to find the switching time-instants t_1, t_2, \dots, t_{2N} in equation (30) by minimizing in certain sense the difference:

$$e(t, t_1, t_2, \dots, t_{2N}) = i_a(t, t_1, t_2, \dots, t_{2N}) - i_{a,1}(t). \quad (40)$$

Namely, the optimal time-domain pulse width modulation problem can be stated as follows: find such time-instants t_1, t_2, \dots, t_{2N} that the following quantity E_2 reaches its minimum value:

$$E_2(t_1, \dots, t_{2N}) = \int_0^{\frac{T}{2}} \left[i_a(t, t_1, \dots, t_{2N}) - I_m \sin\left(\omega t - \phi - \frac{\pi}{6}\right) \right]^2 dt$$

It is apparent that this is the least squares optimization. In mathematical terms, the

latter means the optimization of the error-function $i_a(t) - i_{a,1}(t)$ in the L_2 -norm. It is worthwhile to relate the function $E_2(t_1, \dots, t_{2N})$ to the total harmonic distortion (THD) in phase-current $i_a(t)$. The latter is denoted by THD_I , and it is defined as:

$$THD_I = \frac{\sqrt{\sum_{n=2}^{\infty} I_n^2}}{I_f}, \quad (41)$$

where I_f is the amplitude of the fundamental harmonic component in $i_a(t)$, while I_n is the amplitude of its n^{th} harmonic. It can be easily verified, by substituting $i_a(t, t_1, \dots, t_{2N})$ in (41) in terms of its Fourier series expansion and using the orthogonality property of trigonometric functions that the error integral $E_2(t_1, \dots, t_{2N})$ and THD_I are related by the following equation:

$$E_2(t_1, \dots, t_{2N}) = [(I_f - I_m)^2 + I_f^2(THD_I)^2] \cdot \frac{T}{4}. \quad (42)$$

The last formula is a special case of the well known Parseval's equality for the Fourier series. It is evident from the above formula that the minimization of the function $E_2(t_1, \dots, t_{2N})$ leads to a minimization of the THD in the phase-currents.

It turns out that specific order harmonics in the function $e(t, t_1, \dots, t_{2N})$ defined in (40) can be completely eliminated within the structure of the stated optimization technique. This is done by using constrained optimization. This approach can also be used to ensure that the fundamental harmonic component I_f of the phase-current has the desired value I_m . Namely, the following constraint can be imposed on the switching time-instants that describe the line-voltage $v_{ab}(t)$:

$$\frac{2V_0}{\pi} \sum_{j=1}^{2N} (-1)^{j+1} \cos \omega t_j = V_m, \quad (43)$$

where V_m is defined by formula (39).

Similarly, constraints can be imposed to completely eliminate specific order harmonics. For instance, in order to eliminate the m^{th} harmonic, the following constraint can be used [1, 22, 26]:

$$\sum_{j=1}^{2N} (-1)^j \cos(m\omega t_j) = 0. \quad (44)$$

Thus, the optimization technique can be structured to eliminate specific lower-order harmonics, and minimize the total harmonic content of the remaining higher-order harmonics. It is worthwhile to mention that by using the method of Lagrange multipliers, the stated problem can be reduced to unconstrained optimization.

III. CONSTRAINTS ON SWITCHING TIMES IMPOSED BY SYMMETRIES

A. Symmetries

Symmetries play an important role in pulse width modulation of line-voltages in three-phase inverters. Our subsequent discussion deals with the following symmetries.

S1. Translational Symmetry: The three-phase line-voltages $v_{ab}(t)$, $v_{bc}(t)$ and $v_{ca}(t)$ are time-shifted versions of each other. Namely, the following identity is valid:

$$v_{ab}(t) = v_{bc}\left(t + \frac{T}{3}\right) = v_{ca}\left(t - \frac{T}{3}\right). \quad (45)$$

Translational symmetry ensures that the fundamental harmonic components of the line-voltages form a balanced, positive sequence of three-phase voltages [3]. Furthermore, it can be shown that translational symmetry results in the elimination of all harmonics of orders divisible by three.

S2. Half-Wave Symmetry: This symmetry implies that:

$$v_{ab}(t) = -v_{ab}\left(t + \frac{T}{2}\right). \quad (46)$$

The same half-wave symmetry is valid for $v_{bc}(t)$ and $v_{ca}(t)$. It can be shown that half-wave symmetry results in the elimination of even-order harmonics in the line-voltages.

S3. Quarter-wave symmetry: The objective of PWM is to generate output voltages that approximate ideal sinusoidal voltages. Hence, it makes intuitive sense to impose the following quarter-wave symmetry condition on the PWM voltages:

$$v_{ab}(t) = v_{ab}\left(\frac{T}{2} - t\right). \quad (47)$$

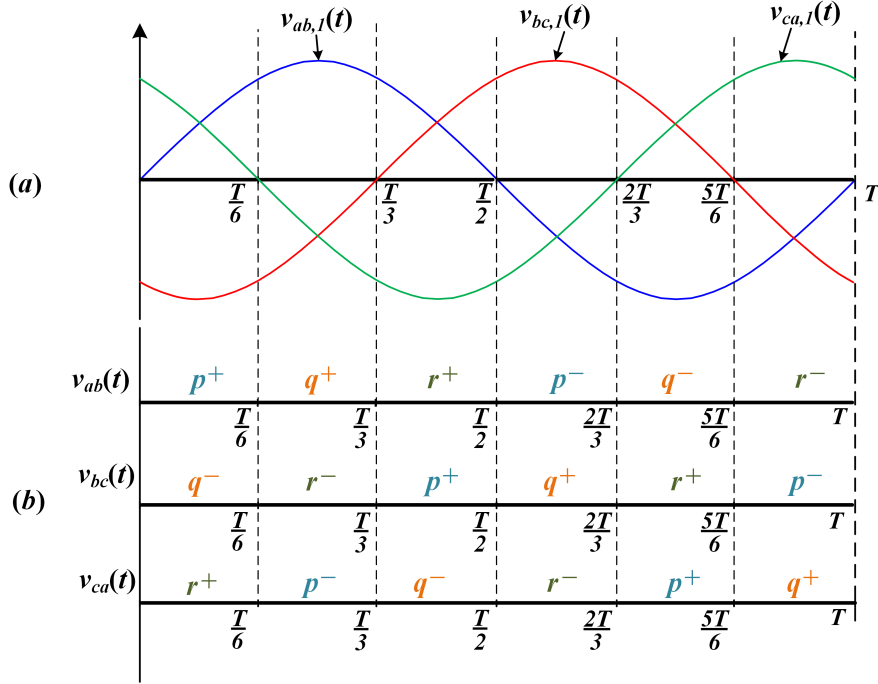


Figure 3: Structure of 3-phase Line-to-line-voltages

It is interesting to point out that quarter-wave symmetry (47), half-wave symmetry (46) and periodicity imply that the line-voltage $v_{ab}(t)$ has odd-symmetry. Indeed:

$$v_{ab}(t) = v_{ab}\left(\frac{T}{2} - t\right) = -v_{ab}(T - t) = -v_{ab}(-t). \quad (48)$$

In addition to the above fundamental symmetry conditions, the three-phase line-voltages must satisfy the following constraints.

C1. KVL constraint: The sum of three-phase line-voltages $v_{ab}(t)$, $v_{bc}(t)$ and $v_{ca}(t)$ equals zero.

$$v_{ab}(t) + v_{bc}(t) + v_{ca}(t) = 0. \quad (49)$$

C2. Switching pattern constraint: These are constraints related to the fact that only the states of the two switches in the same leg of the inverter can be simultaneously changed. This prevents unnecessary switchings and helps minimize switching-losses [1, 16].

B. Role of symmetries on structure of PWM line-voltages

Next, we discuss the implications of the above symmetries and constraints on the structure of the three-phase PWM line-voltages.

The desired fundamental-components of the line-voltages are shown Fig. 3(a). We begin by dividing the interval $0 \leq t \leq T$ into six equal subintervals of length $\frac{T}{6}$. In each of these subintervals, the PWM pulses of the line-voltages can be grouped together to form a *pulse-group*. Thus, for each line-voltage, each subinterval of length $\frac{T}{6}$ can be characterized by a unique pulse-group.

We first describe the pulse-groups that constitute the PWM line-voltage $v_{ab}(t)$. We label these three pulse-groups in the interval $0 \leq t \leq \frac{T}{2}$ as p^+, q^+ and r^+ , respectively. Since $v_{ab,1}(t)$ is positive in the interval $0 \leq t \leq \frac{T}{2}$, $v_{ab}(t)$ shall switch between values 0 and $+V_0$ in this interval, as shown in Fig. 2. Hence, pulse-groups for $v_{ab}(t)$ in the interval $0 \leq t \leq \frac{T}{2}$ are marked by superscript “+”. Furthermore, as a consequence of half-wave symmetry (46), pulses in the interval $\frac{T}{2} \leq t \leq T$ are negative copies of the pulses in $0 \leq t \leq \frac{T}{2}$ (see Fig. 2). Hence, they can be represented by pulse-groups marked using the labels p^-, q^- and r^- , as shown in Fig. 3(b). The pulses that constitute the pulse-groups p^-, q^- and r^- have the same widths but opposite polarities as compared to the corresponding pulses in the p^+, q^+ and r^+ groups, respectively. Thus, p^+, q^+, r^+, p^-, q^- and r^- are six distinct pulse-groups which constitute the line-voltage $v_{ab}(t)$. Furthermore, quarter-wave symmetry (47) for $v_{ab}(t)$ implies the pulses in the p group are mirror images (with respect to $t = \frac{T}{4}$) of those in the r group.

Next, the translational symmetry (45) can be used to determine the pulse-groups in the six subintervals for the line-voltages $v_{bc}(t)$ and $v_{ca}(t)$. Since these line-voltages are time-shifted versions of $v_{ab}(t)$, the pulse-groups in each of the subintervals for $v_{bc}(t)$ and $v_{ca}(t)$ are as shown in Fig. 3(b).

Now, we discuss the implications of the KVL constraint. From Figure 3(b), we observe that in the time interval $0 \leq t \leq \frac{T}{6}$, the line-voltages $v_{ab}(t)$, $v_{bc}(t)$ and $v_{ca}(t)$ have pulses of the p^+, q^- and r^+ groups, respectively. Similarly, for the sub-

sequent time intervals of length $\frac{T}{6}$, the pulse-groups of these three line-voltages are: (q^+, r^-, p^-) , (r^+, p^+, q^-) , (p^-, q^+, r^-) , (q^-, r^+, p^+) and (r^-, p^-, q^+) , respectively. It is apparent that for each of these time intervals, two of the line-voltages are represented by pulses from the p and r groups of the same sign, while the other line-voltage pulses belong to the q group of the opposite sign. Thus, KVL equation (49) as well as the translational symmetry implies that for each pulse in the q^+ (or q^-) group, there are corresponding pulses of the opposite polarity in the p^- (or p^+) group and the r^- (or r^+) group, such that their total sum is equal to zero. Furthermore, since half-wave symmetry ensures that pulses in the q^+ and q^- groups have the same width but opposite signs, we can arrive at the following important conclusion: half-wave symmetry, translational symmetry and the KVL constraint imply that each pulse in the q group is the sum of two specific pulses of the same sign: one from the p group and one from the r group.

C. Constraints on Switching Time-Instants

We now proceed to discuss the constraints that switching time-instants t_1, t_2, \dots, t_{2N} must satisfy to represent three-phase PWM line-voltages.

First, we determine the number of pulses in three-phase PWM line-voltages. Let the number of pulses in the p group be P . Because of quarter-wave symmetry, pulses in the r group are mirror images of pulses in the p group of the same sign. For this reason, the number of pulses in the r group also equals P . Let the number of pulses in the q group be Q . It is apparent from Fig. 3 and KVL that pulses in the q groups must be wider than the pulses in the p and r groups. Furthermore, it was found in the last subsection that pulses in the q group are sums of pulses in the p and r groups of the same sign. This implies that for every pulse in the q group, there must exist one pulse in the p group *and* one pulse in the r group which add to form the given pulse in the q group. This implies that $Q = P$. Thus, we conclude that the number of pulses in the p , q and r groups are the same and equal to P . This means that $N = 3P = 3Q$. It is desirable that $v_{ab}(t = \frac{T}{4}) = V_0$ (since $v_{ab,1}(t)$ reaches maximum at $\frac{T}{4}$). For this reason and quarter-wave symmetry, Q is odd. That is, $Q = 2M + 1$, where M is a natural

number, and hence $N = 3(2M + 1)$.

Next, we proceed to obtain the algebraic relations that the switching time-instants t_1, t_2, \dots, t_{6P} must satisfy in order to represent three-phase PWM line-voltages. Consider the pulses for line-voltage $v_{ab}(t)$ (see Fig. 2) in the interval $0 \leq t \leq \frac{T}{6}$, that is the pulses in the p^+ group. Each such pulse can be indexed by l , where $l = 0, 1, 2, \dots, P$. The switching time-instants associated with the l^{th} pulse in the p^+ group are t_{2l-1} and t_{2l} . Clearly, time-instants $t_{2P+2l-1}$ and t_{2P+2l} correspond to the l^{th} pulse in the q^+ group, while $t_{4P+2l-1}$ and t_{4P+2l} correspond to the l^{th} pulse in the r^+ group.

Our discussion in the previous subsection suggests that switching time-instants for pulses in the q^+ and r^+ groups can be obtained from time-instants t_{2l-1} and t_{2l} in the p^+ group. Indeed, since the pulses in r^+ group are mirror images of those in the p^+ group, the corresponding time-instants for pulses in the r^+ group can be obtained from quarter-wave symmetry. Furthermore, as a consequence of half-wave symmetry, translational symmetry and KVL, each pulse in the q^+ group is the sum of specific pulses in the p^+ and r^+ groups, and hence the time-instants for pulses in the q^+ group can also be obtained in terms of switching time-instants in the p^+ group. We now proceed to derive these relations.

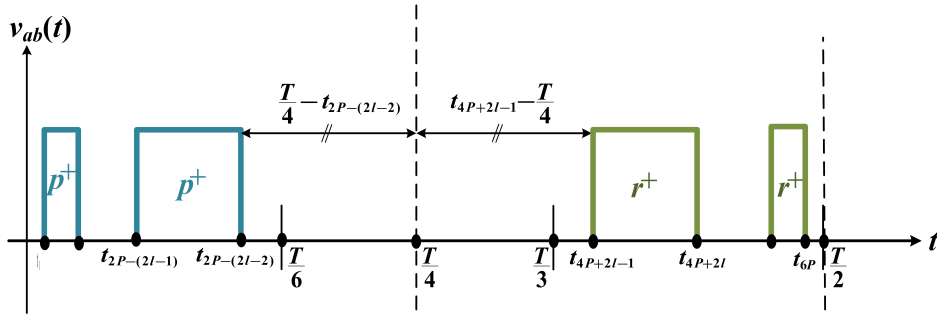


Figure 4: Relation between time-instants in p and r groups

The algebraic relations between switching time-instants for pulses in the p^+ and r^+ groups are easily obtained using the quarter-wave symmetry (47), as shown in Fig. 4. As a consequence of quarter-wave symmetry, for every time-instant defining a rising (falling) edge of a pulse in the p^+ group, there is a corresponding time instant defining a falling (rising) edge of a pulse in the r^+ group, and these two time-instants are related.

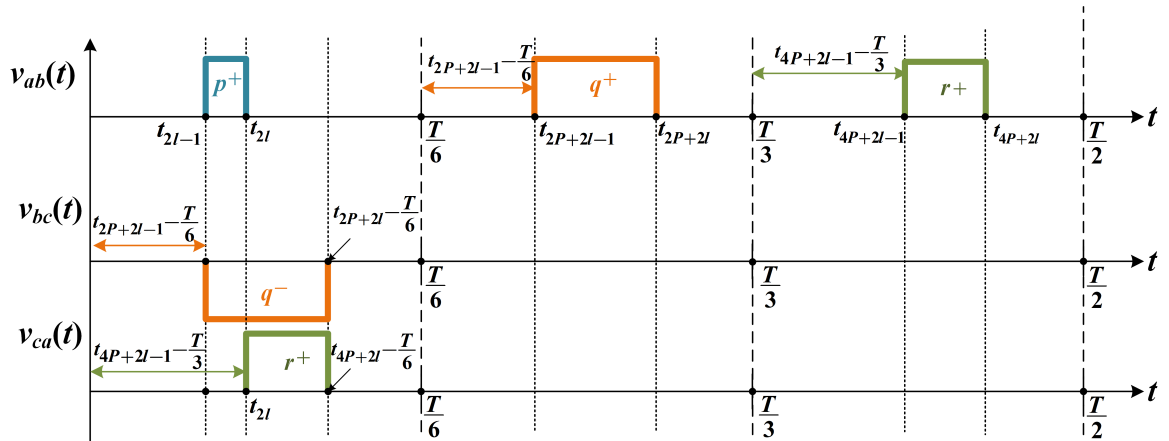


Figure 5: Structure of pulses when $l = \text{odd}$

Thus, for the l^{th} pulse in the p^+ group, the corresponding time-instants for pulses the r^+ group can be obtained as follows:

$$t_{4P+2l-1} = \frac{T}{2} - t_{2P-(2l-2)}, \quad (50)$$

$$t_{4P+2l} = \frac{T}{2} - t_{2P-(2l-1)}, \quad (51)$$

where $t_{2P-(2l-2)}$ and $t_{2P-(2l-1)}$ are time-instants for pulses in p^+ group, and $l = 1, 2, \dots, P$.

We now proceed to obtain switching time-instants for pulses in the q^+ group in terms of switching time-instants in the p^+ group. It can be shown that the single-leg switching constraints (C2) lead to two specific patterns on how the KVL constraint (C1) is realized [1, 2]. Namely, for odd-pulses (i.e. when l is odd), the KVL compensation of the corresponding p , q and r pulses occur as shown in Fig. 5. Whereas, for even-pulses (i.e. when l is even), this compensation occurs as shown in Fig. 6. These figures are used below to derive the formulas for switching time-instants for pulses in the q^+ group in terms of switching time-instants for pulses in the p^+ group. In this way, specific constraints on the switching time-instants for pulses in the p^+ group are also established.

When l is odd, (see Fig. 5), the rising-edge of the pulse in p^+ group corresponds to the rising-edge of the pulse in the q^+ group, the falling-edge of the pulse in the p^+ group corresponds to the rising-edge of the pulse in the r^+ group, while falling-edges of

the pulses in the q^+ and r^+ groups are related. Thus, the time-instant $t_{2P+2l-1}$ in the q^+ group is related to t_{2l-1} in the p^+ group as follows (see Fig. 5):

$$t_{2l-1} = t_{2P+2l-1} - \frac{T}{6}, \quad (52)$$

which leads to

$$t_{2P+2l-1} = t_{2l-1} + \frac{T}{6}, \text{ when } l \text{ is odd.} \quad (53)$$

Similarly, the switching time-instant t_{2P+2l} in the q^+ group is related to t_{4P+2l} in the r^+ group as:

$$t_{2P+2l} - \frac{T}{6} = t_{4P+2l} - \frac{T}{3}. \quad (54)$$

But, using formula (51), we can replace t_{4P+2l} by $\frac{T}{2} - t_{2P-(2l-1)}$, where $t_{2P-(2l-1)}$ is a time-instant in the p^+ group. Thus, the above equation is reduced to:

$$t_{2P+2l} = \frac{T}{3} - t_{2P-(2l-1)}, \text{ when } l \text{ is odd.} \quad (55)$$

Equations (53) and (55) relate time-instants in q^+ group to time-instants in the p^+ group when l is odd.

From Fig. 5, it is also clear that when l is odd, time t_{2l} in the p^+ group and $t_{4P+2l-1}$ in the r^+ group are related. Indeed, from Fig. 5 and using formula (50), we can derive:

$$t_{2l} = t_{4P+2l-1} - \frac{T}{3} = \frac{T}{6} - t_{2P-(2l-2)}, \quad (56)$$

which leads to

$$t_{2l} + t_{2P-(2l-2)} = \frac{T}{6}, \text{ when } l \text{ is odd.} \quad (57)$$

Interestingly, both the switching time-instants t_{2l} and $t_{2P-(2l-2)}$ in equation (57) belong to the p^+ group. This reveals that not all switching time-instants in the p^+ group are completely independent. Instead, there exist among them mutual algebraic relations of the form (57). A similar relation also holds when l is even. This means that the number of independent variables involved in the optimization of the function E_2 needs to be performed is considerably smaller than $2N = 6P$.

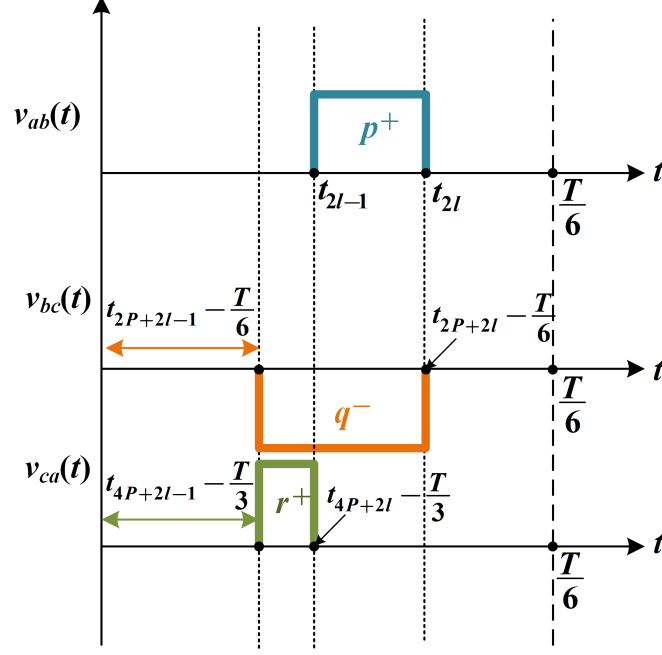


Figure 6: Structure of pulses when $l = \text{even}$

Proceeding in the same way as before, the following equations can be derived when l is even by using Fig. 6:

$$t_{2P+2l-1} = \frac{T}{3} - t_{2P-(2l-2)}, \quad (58)$$

$$t_{2P+2l} = t_{2l} + \frac{T}{6}, \quad (59)$$

$$t_{2l-1} + t_{2P-(2l-1)} = \frac{T}{6}. \quad (60)$$

To summarize, we have established that equations (50), (51), (53), (55), (57), (58), (59) and (60) specify the algebraic relations that the switching time-instants $t_1, \dots, t_{2P}, t_{2P+1}, \dots, t_{4P}, t_{4P+1}, \dots, t_{6P}$ must satisfy to represent three-phase PWM line-voltages with symmetries (S1)-(S3) under the constraints (C1) and (C2). Imposing these relations as equality constraints on the optimization, a symmetry-preserving time-domain PWM optimization technique can be developed. This matter is further discussed in the next section.

IV. SYMMETRY-PRESERVING OPTIMAL PWM AND NUMERICAL RESULTS

In section I, we defined the function E_2 in equation (41) and expressed it as a function of switching time-instants t_1, t_2, \dots, t_{2N} . We discussed how minimizing of E_2 leads to the minimization of the harmonic content of the PWM output current [see equation (42)]. In Section III, we established that $N = 3P$, where P is the number of pulses in each of the p^+ , q^+ and r^+ groups. Using the notation introduced in the previous sections, we can write the objective function as $E_2(t_1, \dots, t_{2P}, t_{2P+1}, \dots, t_{4P}, t_{4P+1}, \dots, t_{6P})$.

We also established that switching time-instants in the q^+ and r^+ groups can be obtained from switching time-instants in the p^+ group, using equations (50),(51),(53), (55), (58) and (59). Moreover, equations (57) and (60) reveal that some switching time-instants in the p^+ group are also related. It can be shown that, when P is odd, there are only $\frac{3P-1}{2}$ independent time-instants, in the sense that with a knowledge of these $\frac{3P-1}{2}$ time-instants, all the $6P$ time-instants can be completely determined using equations (50)-(60). This dramatic reduction in the number of independent variables over which the optimization is performed (from $6P$ to $\frac{3P-1}{2}$) greatly simplifies the numerical computation of the optimization problem.

It is apparent that the time-instants t_1, t_2, \dots, t_{6P} must be strictly monotonically increasing. This constraint can be expressed as the following (non-strict) inequality constraints:

$$t_{j+1} \geq t_j + \tau > t_j, \text{ for all } j = 1, \dots, 6P - 1, \quad (61)$$

and
$$\frac{T}{2} \geq t_{6P} + \tau > t_{6P}, \text{ where } \tau > 0. \quad (62)$$

The inequality constraints in (61) and (62) are used to numerically implement [34–36] the strict monotonicity condition since most numerical optimization solvers do not accept strict inequalities as inputs. It is worthwhile to mention that, if we define:

$$\Delta t_i = t_i - t_{i-1}, \text{ for all } i = 1, \dots, 6P + 1, \quad (63)$$

then, the strict monotonicity constraint can be expressed as:

$$\Delta t_i > 0, \text{ for all } i = 1, \dots, 6P + 1. \quad (64)$$

The latter inequalities define a convex region (cone) [34]. For this reason, it may be advantageous to use the variable Δt_i for numerical minimization.

It is apparent that the optimal PWM depends on the parameters R , L and T . It turns out that this dependence can be expressed in terms of a function of only *one* dimensionless parameter. Indeed, this can be accomplished by introducing the following dimensionless parameter:

$$\alpha = \frac{RT}{L}, \quad (65)$$

and using the scaled-time:

$$\beta = \frac{t}{T}, \quad \left(\beta_j = \frac{t_j}{T}, \text{ for all } j = 1, 2, \dots, 2N \right) \quad (66)$$

as well as voltages:

$$v_{R,ab}(t) = Ri_{ab}(t), \quad (67)$$

$$\tilde{v}_{R,ab}(\beta) = v_{R,ab}(\beta T), \quad (68)$$

$$v_{R,a}(t) = Ri_a(t), \quad (69)$$

$$\tilde{v}_{R,a}(\beta) = v_{R,a}(\beta T), \quad (70)$$

and coefficients

$$B_j = RA_j, \quad \text{for all } j = 1, 2, \dots, 2N + 1. \quad (71)$$

Now, equations (16), (25), (26) and (27), can be rewritten as follows

$$\tilde{v}_{R,ab}(\beta) = \begin{cases} B_{2j+1}e^{-\alpha\beta}, & \text{if } \beta_{2j} < \beta < \beta_{2j+1}, \\ B_{2j+2}e^{-\alpha\beta} + V_0, & \text{if } \beta_{2j+1} < \beta < \beta_{2j+2}, \end{cases} \quad (72)$$

where,

$$B_{2N+1} = V_0 \frac{\sum_{j=1}^{2N} (-1)^j e^{\alpha\beta_j}}{1 + e^{-\frac{\alpha}{2}}}, \quad (73)$$

$$B_1 = -V_0 \frac{\sum_{j=1}^{2N} (-1)^j e^{\alpha\beta_j}}{1 + e^{-\frac{\alpha}{2}}} e^{-\frac{\alpha}{2}}, \quad (74)$$

and

$$B_j = B_1 + V_0 \sum_{n=1}^{j-1} (-1)^n e^{\alpha\beta_n} \quad \text{for } j = 2, 3, \dots, 2N. \quad (75)$$

It is evident that (since $N = 3P$):

$$\tilde{v}_{R,ab}(\beta) = \tilde{v}_{R,ab}(\beta, \beta_1, \dots, \beta_{6P}). \quad (76)$$

Thus, using the formula (69) along with equation (30) and equations (67)-(68), we obtain:

$$\begin{aligned} \tilde{v}_{R,a}(\beta, \beta_1, \dots, \beta_{6P}) &= \frac{1}{3} \left[\tilde{v}_{R,ab}(\beta, \beta_1, \dots, \beta_{6P}) \right. \\ &\quad \left. - \tilde{v}_{R,ab} \left(\beta + \frac{1}{3}, \beta_1, \dots, \beta_{6P} \right) \right]. \end{aligned}$$

It is clear from the above equation that $\tilde{v}_{R,a}(\beta, \beta_1, \dots, \beta_{6P})$ depends only on the parameter α . Similarly, the desired fundamental component of the output voltage $v_{R,a}(t)$ can be expressed as:

$$\tilde{v}_{R,a,1}(\beta) = v_{R,a,1}(\beta T) = V_{R,m} \sin \left(2\pi\beta - \phi - \frac{\pi}{6} \right), \quad (77)$$

where

$$V_{R,m} = \frac{V_m}{\sqrt{3} \sqrt{1 + \frac{4\pi^2}{\alpha^2}}}, \quad (78)$$

and

$$\tan \phi = \frac{2\pi}{\alpha}. \quad (79)$$

If we define the function:

$$\begin{aligned} \tilde{E}_2(\beta_1, \dots, \beta_{6P}) = & \int_0^{\frac{1}{2}} \left[\tilde{v}_{R,a}(\beta, \beta_1, \dots, \beta_{6P}) \right. \\ & \left. - V_{R,m} \sin \left(2\pi\beta - \phi - \frac{\pi}{6} \right) \right]^2 d\beta, \end{aligned}$$

it can be easily verified that

$$\tilde{E}_2(\beta_1, \dots, \beta_{6P}) = \frac{R^2}{T} E_2(t_1, \dots, t_{6P}). \quad (80)$$

Hence, using the above time-scaling, the effects of the parameters R , L and T on the solutions to the optimization problem can be accounted for by using only the parameter α .

Now, the current-harmonics optimization problem in the standard form [34–36] can be stated as follows.

Minimize the function: $\tilde{E}_2(\beta_1, \beta_2, \dots)$ as defined in (80), subject to the strict-monotonicity constraints defined in (61)-(62), as well as constraints (43) and (44) expressed in terms of the β_j variables.

This is the standard problem for constrained non-linear optimization that can be numerically solved using techniques such as Interior Point Methods and Sequential Quadratic Programming [35, 36].

Below, some sample calculations performed by using the mentioned techniques are presented. These calculations have been performed in MATLAB. Interior-Point Method and Sequential Quadratic Programming methods have been used for optimization. In these calculations, the value of the bus voltage V_0 has been taken to be 300 V, and the desired frequency has been chosen to be 60 Hz. The optimization has been performed for different values of inductance L and load resistance R (i.e. for different values of α) as well as for various number of pulses P . Note that P is related to the switching frequency f_{sw} via the following relation:

$$f_{sw} = 6Pf \quad (81)$$

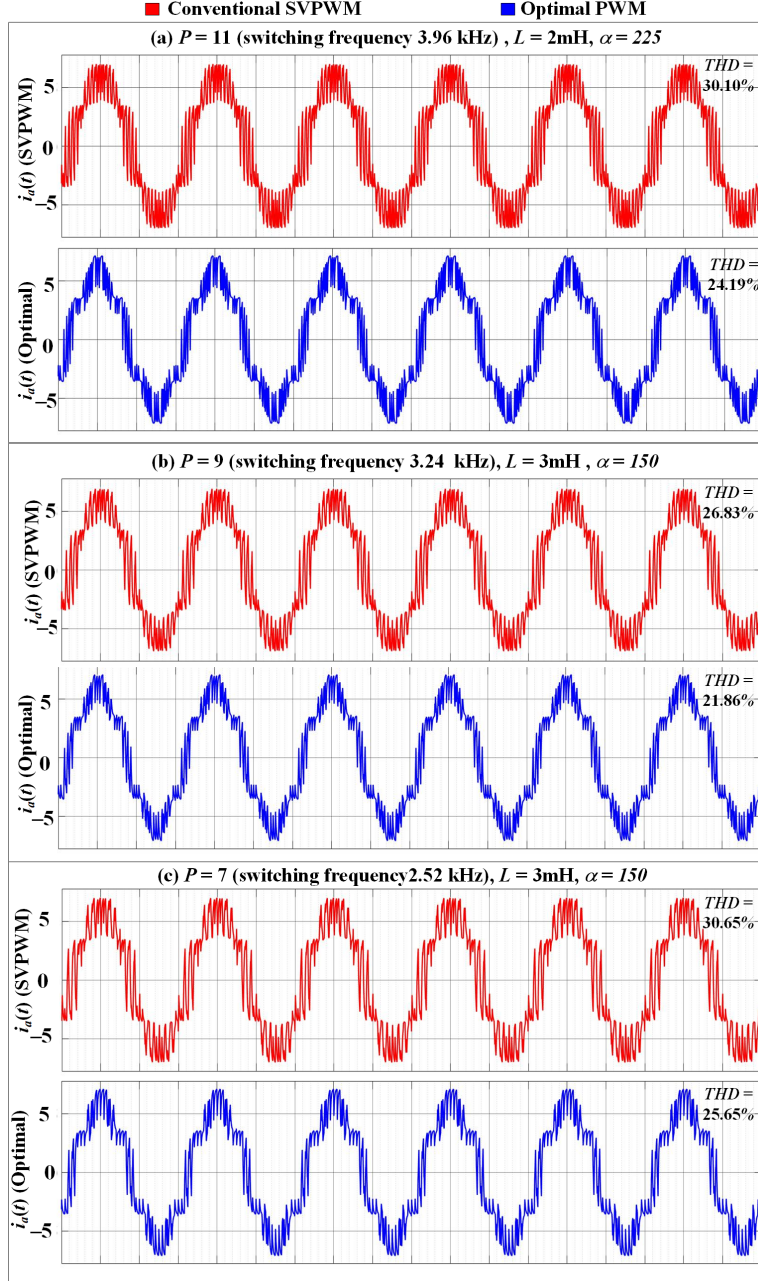


Figure 7: Comparison of conventional SVPWM with Optimal PWM for $I_m = 5A$ and $R = 27\Omega$ and different values of P and L .

where $f = \frac{\omega}{2\pi}$. The initial guess for the switching time-instants has been computed according to the conventional Space Vector PWM (SVPWM). The comparative results of the performed calculations are presented in Fig. 7 and Table 1.

Next, we report the computational results on PWM optimization with elimination of specific lower order harmonics. A major advantage of the time-domain technique is that once the switching time-instants defining PWM voltages are known, exact ampli-

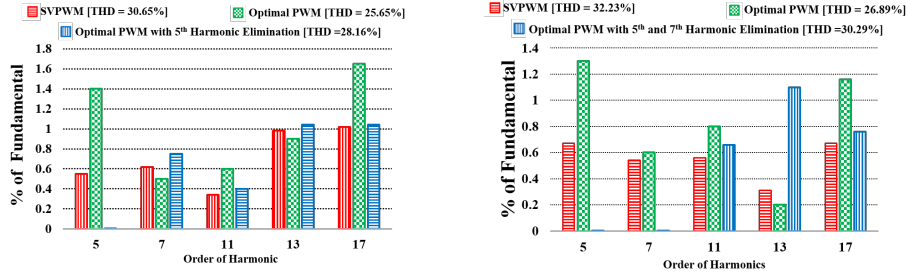
Table 1: Improvement in THD after optimization when $I_m = 5A$ and $R = 27\Omega$

P	f_{sw} (in kHz)	L (in mH)	THD (in %)		% improvement
			SVPWM	Optimal PWM	
5	1.80	5	28.04	23.52	16.12%
7	2.52	3	30.65	25.65	16.17%
9	3.24	3	26.83	21.86	18.52%
11	3.96	2	30.10	24.19	19.63%

tudes of lower-order harmonics can be computed without any approximation. Some of these computations for conventional SVPWM and optimized PWM are shown in Fig. 8. From this figure, it can be seen that in some cases optimization of total harmonic content of the PWM current may result in a slight increase in the percentage of lower-order harmonics. This can be resolved by imposing additional nonlinear constraints of the form (44) on the optimization such that specific lower-order harmonics can be eliminated. It is apparent from this figure that imposing SHE constraints yields sub-optimal performance, as far as THD in the current is concerned. However, even after imposing SHE constraints, better performance than conventional SVPWM, is still achieved in terms of THD.

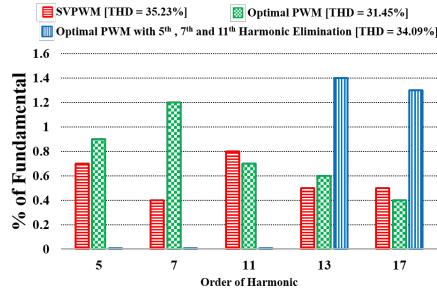
V. CONCLUSION

A per-phase analysis of three-phase inverters is developed and time-domain analytical expressions are derived for the phase-currents in terms of switching time-instants that describe three-phase PWM voltages. Using these analytical expressions, minimization of harmonics in the output currents and voltages is posed as a standard optimization problem. The use of constrained optimization is proposed for selective harmonic elimination. Furthermore, it is demonstrated that three-phase voltage symmetries, KVL and switching patterns impose specific algebraic constraints on switching time-instants of three-phase PWM voltages. This leads to a significant reduction in the number of independent variables over which the optimization is performed. It is worthwhile to stress that the obtained symmetry constraints on switching-time instants of three-phase PWM voltages are of general nature. These constraints can be essential in the design



(a) $P = 7, L = 3 \text{ mH} [\alpha = 150]$

(b) $P = 9, L = 1 \text{ mH} [\alpha = 450]$



(c) $P = 7, L = 1 \text{ mH} [\alpha = 450]$

Figure 8: Computed lower order harmonics for SVPWM, optimal PWM and optimization with the elimination of (a) 5th order harmonic, (b) 5th and 7th order harmonics (c) 5th, 7th and 11th order harmonic for $I_m = 5A$ and $R = 27\Omega$. Values of parameters P, L and α are as specified. Computed THD values are also reported.

of different PWM techniques. In the final section of the paper, it is demonstrated that dependence of the optimized PWM on parameters R, L and T can be expressed in terms of a function of only one dimensionless parameter α by appropriate time-scaling. The numerical results revealing improvements in the harmonic performance of inverters using the optimal time-domain optimization technique are presented. The impact of the optimization on lower-order harmonics is analyzed, and elimination of specific lower-order harmonics using constrained optimization is demonstrated.

References

- [1] D. G. Holmes and T. A. Lipo, *Pulse Width Modulation for Power Converters: Principles and Practice*. Hoboken, NJ: Wiley, 2003.
- [2] Ned Mohan, Tore M. Undeland, William P. Robbins *Power Electronics. Converters, Applications and Design* , John Wiley and Sons, Inc, 2003.
- [3] Isaak D. Mayergoyz, Patrick McAvoy, *Fundamentals of Electric Power Engineering*. World Scientific,2015
- [4] Giuseppe S. Buja, Giovanni B Indri, “Optimal Pulsewidth Modulation for Feeding AC Motors”, *IEEE Trans. Ind. Appl.*, vol. IA-13, no. 1, Jan 1977.
- [5] Jiann-Fuh Chen, Ching-Lung Chu, “Combination voltage-controlled and current-controlled PWM inverters for UPS parallel operation”, *IEEE Trans. Power Electron.*, vol. 10, no. 5, pp. 547-558, 1995.
- [6] J. Holtz, W. Lotzkat, K.-H. Werner, “A high-power multitransistor-inverter uninterruptable power supply system”, *IEEE Trans. Power Electron.*, vol. 3, no. 3, pp. 278-285, 1988.
- [7] J. M. Carrasco, L. G. Franquelo, J. T. Bialasiewicz, E. Galvan, R. C. Portillo Guisado, M. A. M. Prats, J. I. Leon, and N. Moreno-Alfonso, “Power-electronic systems for the grid integration of renewable energy sources: A survey, *IEEE Trans. Ind. Electron.*, vol. 53, no. 4, pp. 10021016, Aug. 2006.
- [8] Y Xue, L Chang, S.B. Kjaer, J Bordonau, T Shimizu, “Topologies of single-phase inverters for small distributed power generators: An overview”, *IEEE Trans. Power Electron.*, vol. 19, no. 5, pp. 13051314, 2004.
- [9] Q Li, P Wolfs, “A review of the single phase photovoltaic module integrated converter topologies with three different DC link configurations”, *IEEE Trans. Power Electron.*,vol 23, no. 3, pp. 13201333, 2008.

- [10] J. Holtz, "Pulsewidth modulation A survey, *IEEE Trans Ind. Electron.*, vol. 39, no. 5, pp. 410-420, Dec. 1992.
- [11] A. Khambadkone and J. Holtz, "Low switching frequency and high dynamic pulsewidth modulation based on field-orientation for high power inverter drive, *IEEE Trans. Power Electron.*, vol. 7, pp. 627-632, 1992.
- [12] J. Shen, S. Schroder, H. Stagge, and R. Doncker, "Impact of modulation schemes on the power capability of high-power converters with low pulse ratios, *IEEE Trans. Power Electron.*, vol. 29, no. 11, pp. 5696-5705, Nov. 2014.
- [13] H.W. van der Broeck, H.-C. Skudelny, G.V. Stanke, "Analysis and Realization of a Pulsewidth Modulator Based on Voltage -Space Vectors," *IEEE Trans. Ind. Appl.*, vol. 24, no. 1, Jan 1988.
- [14] A.H. Bonnett, "Analysis of the impact of pulse-width modulated inverter voltage waveforms on AC induction motors, *IEEE Trans. Ind. Appl.*, vol. 32, pp 386-392, March/April 1996.
- [15] Y. Murai, Y. Gohshi, K. Matsui, and I. Hosono, "High-frequency split zero-vector pwm with harmonic reduction for induction motor drive, *IEEE Trans. Ind. Appl.*, vol. 28, no. 1, pp. 105-112, Jan/Feb 1992.
- [16] D Zhao, VSSPK Hari, G Narayanan, R Ayyanar, "Space-vector-based hybrid pulsewidth modulation techniques for reduced harmonic distortion and switching loss," *IEEE Trans. Power Electron.*, vol. 23, no. 3, pp. 760-774, March 2010.
- [17] A. Tripathi and G. Narayanan, "Investigations on optimal pulse width modulation to minimize total harmonic distortion in the line current, *IEEE Trans. Ind. Appl.*, vol. 53, no. 1, pp. 212-221, Jan. 2017.
- [18] A. Tripathi and G. Narayanan, "Analytical Evaluation and Reduction of Torque Harmonics in Induction Motor Drives Operated at Low Pulse Numbers", *IEEE Trans. Ind. Electron.*, May 2018.

- [19] T. Bruckner and D. G. Holmes, "Optimal pulse-width modulation for three-level inverters, *IEEE Trans. Power Electron.*, vol. 20, no. 1, pp. 8289, Jan. 2005.
- [20] W. Chen, H. Sun, X. Gu, and C. Xia, "Synchronized space-vector PWM for three-level VSI with lower harmonic distortion and switching frequency, *IEEE Trans. Power Electron.*, vol. 31, no. 9, pp. 64286441, Sep. 2016.
- [21] A. Beig, S. Kanukollu, K. Al Hosani, and A. Dekka, Space-vector-based synchronized three-level discontinuous PWM for medium-voltage highpower VSI, *IEEE Trans. Ind. Electron.*, vol. 61, no. 8, pp. 38913901, Aug. 2014
- [22] F. G. Turnbull, Selected harmonic reduction in static dc-ac inverters, *IEEE Trans. Commun. Electron.*, vol. CE-83, pp. 374378, Jul. 1964.
- [23] H. S. Patel and R. G. Hoft, "Generalized techniques of harmonic elimination and voltage control in thyristor inverters: Part 1 Harmonic elimination, *IEEE Trans. Ind. Appl.*, vol. IA-9, no. 3, pp. 310317, May/Jun. 1973.
- [24] P. N. Enjeti, P. D. Ziogas, and J. F. Lindsay, Programmed PWM techniques to eliminate harmonics: a critical evaluation, *IEEE Trans. Ind. Applicat.*, vol. 26, pp. 302316, Mar./Apr. 1990.
- [25] H. R. Karshenas, H. A. Kojori, and S. B. Dewan, Generalized techniques of selective harmonic elimination and current control in current source inverters/converters, *IEEE Trans. Power Electron.*, vol. 10, pp. 566573, Sept. 1995.
- [26] D. Czarkowski, D. V. Chudnovsky, G. V. Chudnovsky, and I. W. Selesnick, "Solving the optimal PWM problem for single-phase inverters, *IEEE Trans. Circuits Syst. I*, vol. 49, no. 4, pp. 465475, Apr. 2002.
- [27] J. N. Chiasson, L. M. Tolbert, K. J. McKenzie, and Z. Du, "A complete solution to the harmonic elimination problem, *IEEE Trans. Power Electron.*, vol. 19, no. 2, pp. 491499, Mar. 2004.

- [28] J. R. Wells, B. M. Nee, P. L. Chapman, and P. T. Krein, Selective harmonic control: a general problem formulation and selected solutions, *IEEE Trans. Power Electron.*, vol. 20, no. 6, pp. 13371345, Nov. 2005.
- [29] J. R. Wells, X. Geng, P. L. Chapman, P. T. Krein, and B. M. Nee, “Modulation-based harmonic elimination, *IEEE Trans. Power Electron.*, vol. 22, no. 1, pp. 336340, Jan. 2007.
- [30] J. Napoles, J. Leon, R. Portillo, L. Franquelo, and M. Aguirre, “Selective harmonic mitigation technique for high-power converters, *IEEE Trans. Ind. Electron.*, vol. 57, no. 7, pp. 23152323, Jul. 2010.
- [31] E. Twining and D. G. Holmes, “Grid current regulation of a three-phase voltage source inverter with an LCL input filter, *IEEE Trans. Power Electron.*, vol. 18, no. 3, pp. 888895, May 2003.
- [32] N. Oikonomou and J. Holtz, “Closed-loop control of medium-voltage drives operated with synchronous optimal pulsewidth modulation, *IEEE Trans. Ind. Appl.*, vol. 44, no. 1, pp. 115123, Jan/Feb 2008.
- [33] I. Mayergoyz and S. Tyagi, “Optimal time-domain technique for pulse-width modulation in power electronics,” *AIP Advances*, vol. 8, no. 5, May 2018.
- [34] Y. Nesterov, *Introductory Lectures on Convex Optimization*. Kluwer Academic Publishers, Norwell, MA (2004)
- [35] R.H. Byrd, Mary E. Hribar, and Jorge Nocedal, “An Interior Point Algorithm for Large-Scale Nonlinear Programming,” *SIAM Journal on Optimization*, vol 9, no. 4, pp. 877900, 1999.
- [36] J. Nocedal and S. J. Wright, *Numerical Optimization, Second Edition*. Springer Series in Operations Research, Springer Verlag, 2006.